ECS Transactions, 50 (9) 363-370 (2012)

Strain Engineering for Optical Gain in Germanium

M. El Kurdi[a], M. de Kersauson[a], A. Ghrib[a], M. Prost[a,d], S. Sauvage[a], R. Jakomin[b], G. Beaudoin[b], O. Mauguin[b], L. Largeau[b], I. Sagnes[b], G. Ndong[c], M. Chaigneau[c], R. Ossikovski[c,], P. Boucaud[a]

[a] Institut d'Electronique Fondamentale, CNRS-Université Paris Sud, F-91405 Orsay, France
[b] Laboratoire de Photonique et de Nanostructres, CNRS-UPR20, Route de Nozay, 91460 Marcoussis, France
[c] Laboratoire de Physique des Interfaces et des Couches Minces, CNRS-Ecole polytechnique, 91128 Palaiseau Cedex, France
[d] STMicroelectronics, 850 rue Jean Monnet 38920 Crolles, France

Room temperature optical gain and lasing have been recently demonstrated in germanium. One key ingredient to obtain positive gain is to reduce the splitting between the conduction indirect and direct valleys by introducing tensile strain. We have investigated two distinct approaches to apply a large tensile strain in germanium. The first approach relies on the growth of germanium on InGaAs buffer templates. Biaxial tensile strains up to 0.8% have been achieved by this method. The second approach relies on stress transfer through silicon nitride layers. It offers the advantage of a full compatibility with CMOS processing. We have successfully fabricated tensile-strained photonic wires which exhibit optical gain under cw optical pumping.

Introduction

The integration of an optical source on silicon represents a major challenge for CMOS compatible data transfer and more generally for the development silicon photonics. One prerequisite for the successful integration of a source is obviously the compatibility with silicon processing environment. However, the performances of the source need to reach those of standard III-V counterparts in order to represent a viable alternative as compared to heterogeneous integration. Lasing has been recently demonstrated for germanium grown on silicon, either under optical pumping[1] or more recently under electrical injection.[2] A promising route to enhance the performances of such lasers is to increase the tensile strain, either biaxial or uniaxial, in the germanium film.[3,4,5] The tensile strain decreases the energy splitting between the L valley and the zone-center Gamma valley. It thus leads to a more efficient population of the Brillouin zone-center Gamma valley where the carriers can optically recombine efficiently. A direct band gap corresponding to the situation where the minimum of the conduction band is given by the zone center valley is expected to occur for a biaxial tensile strain around 2%. Simultaneously, the tensile strain lifts the valence band degeneracy between heavy hole and light hole by pushing the light hole band at higher energy. Depending on the amount of tensile strain, both light hole and heavy hole bands might contribute to the optical gain leading to a

broad spectral range where gain is present. The amplitude of tensile strain is however not the only parameter of interest. There is a trade-off between the thickness of the germanium and the amount of tensile strain that can be sustained. Very large tensile strain, up to 2%, have been achieved but on very thin germanium nanomembranes.[6,7] These membranes might however be too thin to exhibit a significant modal optical gain. It is therefore necessary to investigate carefully the relationship between strain and film thickness. Several methods are available to transfer a tensile stress into a germanium film. The mechanical deformation approach is interesting[6,8,9] but is probably too challenging for a laser integration on chip. Another approach relies on the heteroepitaxial growth on a buffer layer with a larger lattice parameter than bulk germanium. This can be achieved by growth on germanium-tin alloys[10] or on InGaAs buffer layers.[11,12,13] The stress transfer using silicon nitride layers is also an attractive option as it is flexible and fully compatible with CMOS processing. In this article, we review the recent results that we have obtained for germanium growth on InGaAs buffer layers and the stress transfer in germanium waveguides using silicon nitride stressors.

Growth of germanium on InGaAs buffers

The germanium films and InGaAs buffers are grown by metalorganic chemical vapor deposition (MOCVD) on GaAs substrates. Growth on germanium on GaAs substrate allows one to obtain a high quality germanium film as both materials are nearly lattice-matched. The same MOCVD chamber can handle both III-V and group IV elements and the growth is performed at low pressure (70 Torr) using dihydrogen as carrier gas. Ge growth was obtained by using isobutyl-germane as metal-organic precursor.[2] Trimethyl-indium, trimethyl-gallium and arsine were used for III-V elements. The thickness of the InGaAs buffer layers is 1 μm. Their amount of plastic relaxation is around 90%. This plastic relaxation was measured by X-ray diffraction. The samples were probed by room temperature photoluminescence. The luminescence was excited using either a cw 532 nm laser or a 632.8 nm He-Ne laser.[14,15] The luminescence was dispersed by 50 cm focal length spectrometer and an extended InGaAs photodetector array.

Figure 1 (a) shows the room temperature photoluminescence spectra of 150 nm thick germanium films grown on InGaAs buffer layers with various indium content. The luminescence is measured for an excitation-collection at normal incidence using the same objective. The luminescence is dominated by the direct band gap recombination that gradually shifts towards long wavelength (i.e. low energy) as the indium content is increased. The doping of the germanium film contributes also to a red-shift of the emission as compared to bulk undoped germanium.[16] For an effective indium content of 13%, the photoluminescence maximum is red-shifted by 140 nm as compared to bulk germanium on GaAs, corresponding to a biaxial strain of 0.77%. The linewidth of the emission also increases as the indium content increases and is characterized by an increased broadening at low energy. We attribute this broadening to the change of ratio between direct band gap and indirect band gap recombination. This ratio is sensitive to non-radiative recombination rates[17] and we observe a continuous increase of the ratio between indirect band gap amplitude/direct band gap amplitude. The amplitude of the indirect band gap photoluminescence amplitude can be as large as the one of the direct band gap for the high-strain layer. We have compared the dependence of the photoluminescence maximum with the one calculated using a multi-band **k.p** formalism.[18,19,4] The equivalent indium content accounts for the partial relaxation of the InGaAs buffer that is around 90%. The comparison is shown in Fig. 1 (b). Both

dependences of heavy hole and light hole bands are considered. The recombination is unambiguously attributed to a mechanism involving the zone center conduction band and the heavy hole valence band.

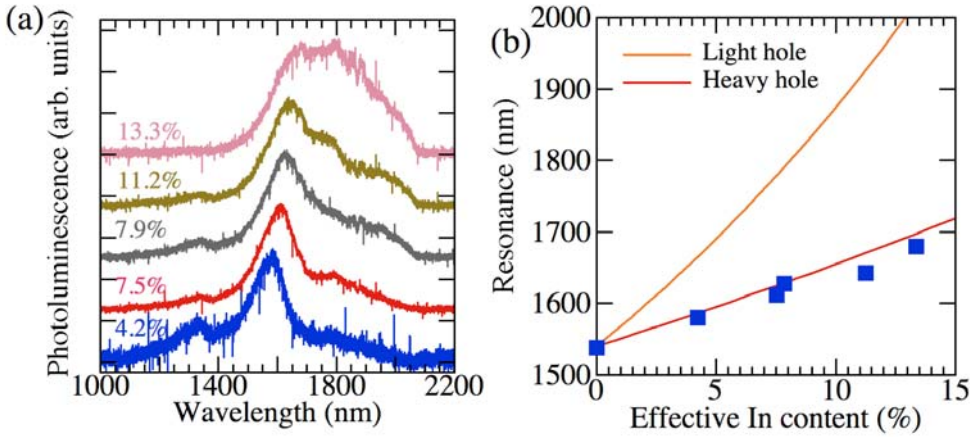

Figure 1. (a) Room temperature photoluminescence for a 150 nm thick germanium film grown on InGaAs buffer layers with various indium content. The equivalent indium content accounts for the partial relaxation of the buffer layer. The curves have been normalized and offset for clarity. The luminescence is excited by a He-Ne laser. The small resonance at 1330 nm is a defect signal from the InGaAs buffer layer. (b) Comparison between the resonance wavelength of the direct band gap recombination and the one calculated using a 30 band **k.p** formalism. The calculated positions of recombination involving heavy hole and light hole are indicated as full lines. The squares correspond to the experimental data.

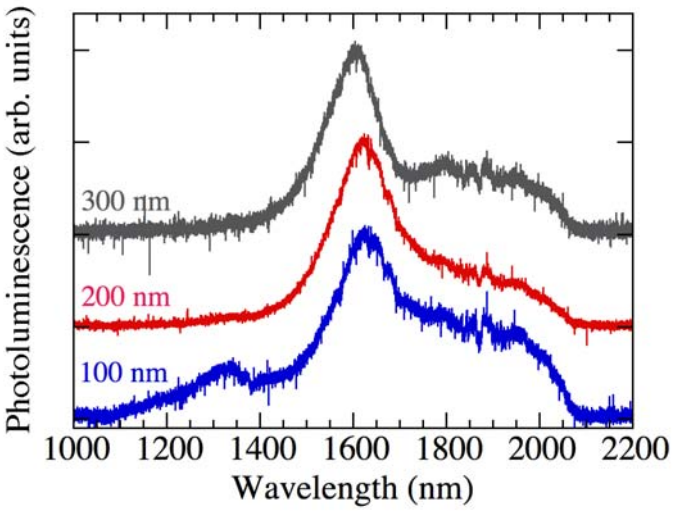

Figure 2. Room temperature photoluminescence of tensile-strained Ge layers with different thicknesses grown on an InGaAs buffer. The InGaAs buffer layer has an indium content of 9.8% as measured by X-ray diffraction. The curves have been normalized and offset for clarity. The Ge thickness is indicated in the figure. The small resonance at 1330 nm clearly observed on the 100 nm thick layer is a defect signal from the InGaAs buffer layer. The luminescence is excited by a He-Ne laser.

Figure 2 shows the dependence of the room temperature photoluminescence as a function of the thickness of the germanium film. The indium content of the buffer layer is 9.8%. The equivalent biaxial strain is 0.47% for small thicknesses of the germanium layer with a direct band gap photoluminescence maximum around 1629 nm. A red-shift of the photoluminescence is observed for thicknesses larger than 200 nm. This red-shift is a signature of partial relaxation of the film. From the energy position of the photoluminescence maximum, we deduce that the biaxial strain decreases from 0.47% to 0.34% for the 300 nm thick sample. This partial relaxation is also associated with an increase of non-radiative recombination as the amplitude decreases by a factor of 2 for the 300 nm thick sample as compared to the 200 nm thick sample. These measurements indicate that significant biaxial strain can be obtained on structures with a thickness that are compatible with optical waveguiding.

Stress transfer through silicon nitride layers

Another approach to transfer stress into a germanium is the use of silicon nitride layers. This technique is widely used in the microelectronics industry for transistor mobility enhancement. The deposition of a silicon nitride layer offers the advantage of a full compatibility with CMOS processing. In order to induce a tensile strain in the germanium layer, a compressively-strained Si_3N_4 layer is deposited by plasma-enhanced chemical vapor deposition on germanium ridge waveguides. The Si_3N_4 layer being free to move, the stored energy relaxes by lateral displacement inducing a stress transfer in the germanium layer.[20,21] Figure 3 (a) shows a schematic description of the investigated structure. A 500 nm thick germanium layer was first grown on a GaAs substrate by MOCVD. Ridge waveguides with various widths are defined by etching the germanium film. A second etching step is performed in order to vertically etch the GaAs substrate down to a 1.2 µm depth. This second step avoids the transfer of compressive strain that is present at the bottom edge of the waveguide after nitride deposition. The silicon nitride is then deposited by plasma-enhanced chemical vapor deposition. Depending on the deposition parameters, different stress amplitudes can be obtained in the nitride layer. In the following, we have investigated nitride films with equivalent hydrostatic stess values used in the modeling of 3 and 4.5 GPa. Figure 3 (b) shows a cross section scanning electron microscope image of a structure fabricated with this method.

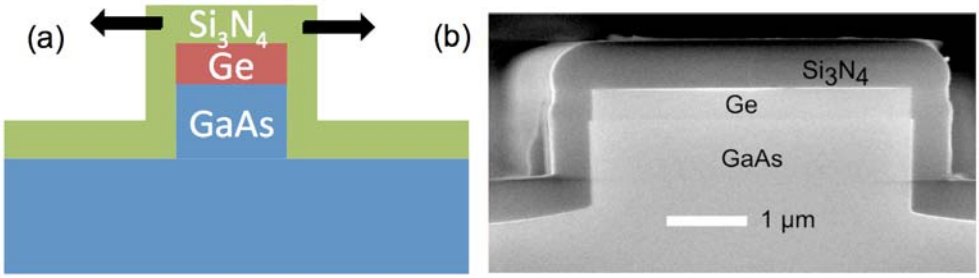

Figure 3. (a) Schematic drawing of stress transfer into germanium waveguides using a strained silicon nitride layer. The *x* direction is perpendicular to the ridge long axis. (b) Scanning electron microscope image of the fabricated structure. The thickness of the nitride layer is 600 nm. The thickness of the germanium film is 500 nm.

We have investigated the stress transfer into the germanium waveguide by spatially-resolved microRaman spectroscopy. Under the assumption of biaxial or uniaxial plane

stress, the Raman shift provides an information on the strain field close to the surface. The investigated germanium waveguide is 4 µm wide. Figure 4 (a) shows the spatial dependence of the strain component ε_{xx} as measured by Raman spectroscopy. Figure 4 (b) shows the calculated finite element strain profile. An initial 3 GPa hydrostatic stress in the nitride layer was considered in the modeling. A very good agreement is obtained between experiment and modeling, in particular at the waveguide center. The situation becomes more complex at the edge. At the center of the waveguide, Raman indicates a 0.62% uniaxial strain component. The strain modeling provides a 0.7% value. We emphasize that the value deduced by Raman is based on the assumption of uniaxial or biaxial in-plane strain without shear. Therefore, it does not account for the possible presence of shear components (e.g. $\varepsilon_{xy} \neq 0$) that can be expected at the waveguide edge. Further, if the strain is strictly uniaxial, i.e. $\varepsilon_{yy} = 0$, then the strain value obtained equals ε_{xx} as expected; however, if the strain is biaxial, i.e. $\varepsilon_{yy} \neq 0$ e.g. because of residual strain in the Ge layer due to the Ge/GaAs lattice mismatch, then the strain value is the sum of ε_{xx} and ε_{yy}. These facts tentatively explain the slight difference that remains within 10% deviation. The average value of ε_{xx} deduced by Raman in a 2 µm window around the center is 0.69%.

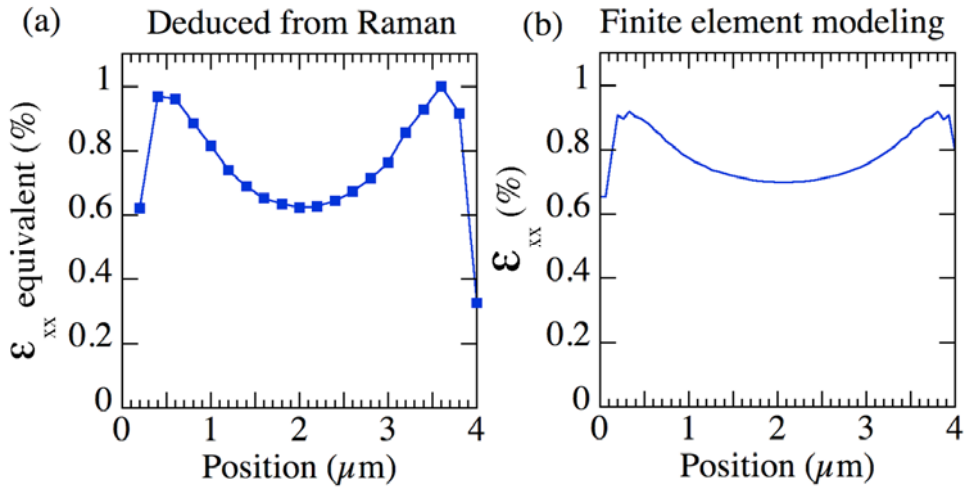

Figure 4. (a) Strain profile ε_{xx} as deduced from Raman measurement under the assumption of uniaxial plane stress for a 4 µm wide germanium waveguide. (b) Strain profile as obtained from finite element modeling. At waveguide center, $\varepsilon_{xx} = 0.62$ % is deduced from Raman. The average value of ε_{xx} deduced by Raman in a 2 µm window around the center is 0.69 %.

The stress transfer is strongly dependent on the width of the waveguides. For very large waveguides, no stress transfer is expected. On the contrary, there is a limit to strain amplitude before the onset of plastic relaxation or formation of cracks. We have investigated this size dependence by room temperature photoluminescence measured at the waveguide center by microphotoluminescence. Figure 5 (a) shows the dependence for films initially strained by a 4.5 GPa nitride stress. As the width of the waveguide is reduced, the photoluminescence shifts to longer wavelength, indicating an increase of the stress transfer. We have modeled this dependence by combining the calculated strain profile obtained by finite element and the calculation of the germanium electronic band structure as obtained with a 30 band **k.p** formalism. The calculated photoluminescence

spectra are superimposed on the experimental results. The calculation does not account for the indirect band gap recombination which explains the discrepancy at long wavelength. A good agreement is obtained between modeling and experiments for the photoluminescence maximum. An uniaxial strain ε_{xx} of 1.07 % is deduced from the photoluminescence spectra. This value is very encouraging as it indicates that significant stress can be transferred into germanium, thus opening the possibility to reduce the threshold to achieve lasing.

The stress amplitude is not the only factor that influences the carrier recombination at zone center. The orientation of the waveguide is also important. For waveguides oriented along <110> direction, the strain induces a splitting of the L valley. This splitting is not present for waveguides oriented along <100> direction. The splitting of the L valley reduces the efficiency of carrier transfer into the zone center Gamma valley. Therefore, one expects a weaker photoluminescence for waveguides oriented along <110> directions as compared to <100> direction. The effect should also be more pronounced as the strain in the waveguide increases. Figure 5 (b) shows an experimental illustration of this effect. The photoluminescence spectra are very similar between both orientations for the 8 µm width waveguide. As the width is reduced, the photoluminescence amplitude difference increases, with a significant larger value for <100> oriented waveguides. This change of amplitude is well correlated with the modeling of the zone center electron population (not shown).

Another method to fabricate tensile-strained germanium wires is to use the nitride layers as a hard mask for germanium etching. This approach was illustrated in Ref. 21. An uniaxial strain of 0.6% was achieved in the latter case. The photoluminescence spectra of germanium photonic wires fabricated by this method have been investigated for an optical pumping along the wire length. The experimental results were reported in Ref. 21. Optical gain around 1680 nm has been observed using a variable stripe length method. It demonstrates that lasing can be expected for germanium wires tensily-strained by a silicon nitride layer.

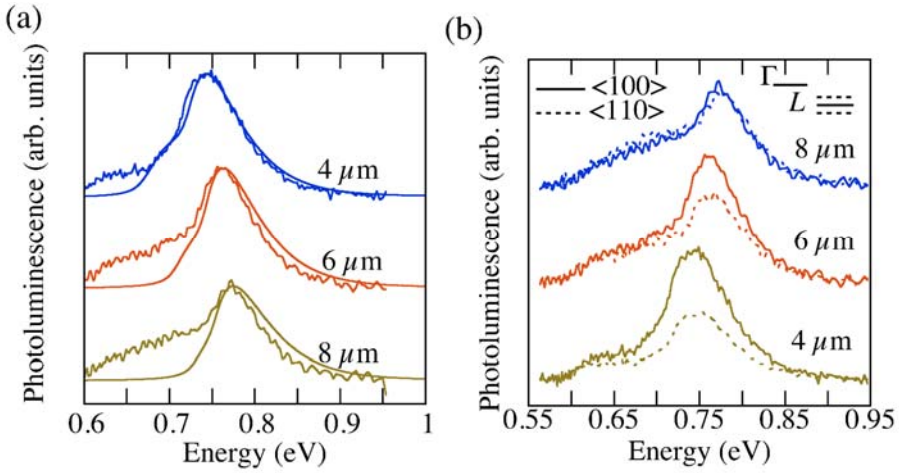

Figure 5. (a) Room temperature photoluminescence spectra for variable germanium waveguide widths. The smooth lines correspond to the modeling. The initial hydrostatic stress in the nitride film is 4.5 GPa. (b) Room temperature photoluminescence spectra for samples with variable widths and distinct orientations. The thick lines correspond to the <100> ridge direction. The dashed lines correspond to the <110> direction. The curves have been offset for clarity.

Conclusion

We have illustrated two distinct approaches to induce a tensile strain into a germanium film. The first approach relies on the growth on a buffer layer with a larger lattice constant like InGaAs. Significant biaxial tensile strain can be obtained for germanium layer thicknesses that are compatible for optical waveguiding. The second approach is based on the stress transfer using silicon nitride layers. The efficiency of stress transfer depends on the stress in the nitride and on the waveguide width. Uniaxial strain up to 1% has been demonstrated in germanium waveguide. The orientation of the waveguide also plays a crucial role with a more efficient zone center population for waveguides oriented along <100> direction. The achievement of large strain in germanium waveguides should allow to decrease the threshold for lasing.

Acknowledgments

This work was supported by “Triangle de la Physique” under Gerlas convention and by Agence Nationale de la Recherche under GRAAL convention (ANR Blanc call 2011 BS03 004 01).

References

1. J. Liu, X. Sun, R. Camacho-Aguilera, L. C. Kimerling, and J. Michel, *Opt. Lett*. **35**, 679 (2010).
2. R. E. Camacho-Aguilera, Y. Cai, N. Patel, J. T. Bessette, M. Romagnoli, L. C. Kimerling, and J. Michel, *Opt. Express* **20**, 11316 (2012).
3. J. Liu, X. Sun, D. Pan, X. Wang, L. C. Kimerling, T. L. Koch, and J. Michel, *Opt. Express* **15**, 11272 (2007).
4. M. El Kurdi, G. Fishman, S. Sauvage, and P. Boucaud, *J. Appl. Phys.* **107**, 013710 (2010).
5. G. Pizzi, M. Virgilio, and G. Grosso, *Nanotechnology* **21**, 055202 (2010).
6. J. R. Sanchez-Perez, C. Boztug, F. Chen, F. F. Sudradjat, D. M. Paskiewicz, R. Jacobson, M. G. Lagally, and R. Paiella, *Proc. Natl. Acad. Sci.* **108**, 18893 (2011).
7. Y. Huo, H. lin, R. Chen, M. Marakova, Y. Rong, M. Li, T. I. Kamins, J. Vuckovic, and J. S. Harris, *Appl. Phys. Lett.* **98**, 011111 (2011).
8. M. El Kurdi, H. Bertin, E. Martincic, M. de Kersauson, G. Fishman, S. Sauvage, A. Bosseboeuf, and P. Boucaud, *Appl. Phys. Lett.* **96**, 041909 (2010).
9. P. Lim, S. Park, Y. Ishikawa, K. Wada, *Opt. Exp*. **17**, 16358 (2009).
10. J. Menendez and J. Kouvetakis, *Appl. Phys. Lett.* **85**, 1175 (2004).
11. Y. Bai, K. E. Lee, C. Cheng, M. L. Lee, and E. A. Fitzgerald, *J. Appl. Phys.* **104**, 084518 (2008).
12. R. Jakomin, M. de Kersauson, M. El Kurdi, L. Largeau, O. Mauguin, G. Beaudoin, S. Sauvage, R. Ossikovski, G. Ndong, M. Chaigneau, I. Sagnes, and P. Boucaud, *Appl. Phys. Lett.* **98**, 091901 (2011).
13. Y. Hoshina, A. Yamanda, and M. Konagai, *Jpn. J. Appl. Phys*. **48**, 111102 (2009).

14. P. Boucaud, S. Sauvage, M. Elkurdi, E. Mercier, T. Brunhes,V. Le Thanh, D. Bouchier, O. Kermarrec, Y. Campidelli, D. Bensahel, *Phys. Rev. B* **64**, 155310 (2001).
15. S. David, M. El Kurdi, P. Boucaud, A. Chelnokov, V. Le Thanh, D. Bouchier, J.-M. Lourtioz, *Appl. Phys. Lett.* **83**, 2509 (2003).
16. M. El Kurdi, T. Kociniewski, T.-P. Ngo, J. Boulmer, D. Debarre, P. Boucaud, J. F. Damlencourt, O. Kermarrec, and D. Bensahel, *Appl. Phys. Lett.* **94**, 191107 (2009).
17. G. Grzybowski, R. Roucka, J. Mathews, L. Jiang, R. T. Beeler, J. Kouvetakis, and J. Menendez, *Phys. Rev. B* 84, 205307 (2011).
18. M. El Kurdi, G. Fishman, S. Sauvage, and P. Boucaud, *Phys. Rev. B* **68**, 165333 (2003).
19. M. El Kurdi, S. Sauvage, G. Fishman, and P. Boucaud, *Phys. Rev. B* **73**, 195327 (2006).
20. A. Ghrib, M. de Kersauson, M. El Kurdi, R. Jakomin, G. Beaudoin, S. Sauvage, G. Fishman, I. Sagnes, P. Boucaud, *Appl. Phys. Lett.* **100**, 201104 (2012).
21. M. de Kersauson, M. El Kurdi, S. David, X. Checoury, G. Fishman, S. Sauvage, R. Jakomin, G. Beaudoin, I. Sagnes, and P. Boucaud, *Opt. Express* **19**, 17925 (2011).